Biol Cybern (2008) 98:479–490
DOI 10.1007/s00422-008-0218-0

ORIGINAL PAPER

Biological Cybernetics

Electric field interactions in pairs of electric fish: modeling and mimicking naturalistic inputs

Marc Kelly · David Babineau · André Longtin · John E. Lewis

Received: 10 November 2007 / Accepted: 21 January 2008

Abstract Weakly electric fish acquire information about their surroundings by detecting and interpreting the spatial and temporal patterns of electric potential across their skin, caused by perturbations in a self-generated, oscillating electric field. Computational and experimental studies have focused on understanding the electric images due to simple, passive objects. The present study considers electric images of a conspecific fish. It is known that the electric fields of two fish interact to produce beats with spatially varying profiles of amplitude and phase. Such patterns have been shown to be critical for electrosensory-mediated behaviours, such as the jamming avoidance response, but they have yet to be well described. We have created a biophysically realistic model of a wave-type weakly electric fish by using a genetic algorithm to calibrate the parameters to the electric field of a real fish. We use the model to study a pair of fish and compute the electric images of one fish onto the other at three representative phases within a beat cycle. Analysis of the images reveals rostral/caudal and ipsilateral/contralateral patterns of amplitude and phase that have implications for localization of conspecifics (both position and orientation) and communication between conspecifics. We then show how the common stimulation paradigm used to mimic a conspecific during in vivo electrophysiological experiments, based on a transverse arrangement of two electrodes, can be improved in order to more accurately reflect the important qualitative features of naturalistic inputs, as revealed by our model.

Keywords Electrosensory system · Weakly electric fish · Finite-element modeling

M. Kelly · D. Babineau · A. Longtin
Department of Physics, University of Ottawa,
Ottawa, ON KIN 6N5, Canada

M. Kelly · J. E. Lewis (✉)
Department of Biology, University of Ottawa,
30 Marie-Curie, Ottawa, ON K1N 6N5, Canada
e-mail: john.lewis@uottawa.ca

M. Kelly · D. Babineau · A. Longtin · J. E. Lewis
Center for Neural Dynamics, University of Ottawa,
Ottawa, ON KIN 6N5, Canada

1 Introduction

Most object localization problems involve well-understood sensory inputs, related for example to variations in light intensity in the case of vision, or interaural time and intensity differences in the case of audition. The problem of object localization thus lies primarily in understanding how the nervous system encodes and performs computations on these sensory inputs. This is not yet the case for the electrosensory systems of weakly electric fish—although electric fish are a great model system for investigating sensory signal processing, we still have much to learn about the naturalistic spatiotemporal inputs that these fish use to communicate and localize objects in the dark.

Wave-type weakly electric fish use a specialized electric organ to generate an oscillating dipole-like electric field that surrounds their body, called the *electric organ discharge (EOD)*. Nearby objects having conductivities different than that of the water (rocks, plants, prey, etc.), as well as other fish, perturb the EOD and generate a virtual field, called the *perturbing field* (and strictly defined as the difference in the EOD with and without the object) (Caputi and Budelli 2006) that results in spatiotemporal patterns of voltage difference across their skin, called the *electric image*. Specialized skin electroreceptors encode the electric image and send the information to the brain. In order to understand electrosensory object localization, we must first understand the associated electric images.

The electric images of some simple objects have been well studied. Objects that are small (in relation to the spatial variation of the EOD) and have similar length scales in all dimensions, will produce a perturbing field similar to the field of a dipole, oriented parallel to the direction of the local electric field. These simple objects, such as spheres or cubes, are known to produce a mexican-hat-shaped electric image, whose peak location, amplitude and width vary systematically with object location relative to the fish for a fixed phase of the EOD cycle (von der Emde 1999; Chen et al. 2005; Babineau et al. 2006; Caputi and Budelli 2006). Thus, the electric image contains all the information necessary to localize such objects in 3-dimensions (Rasnow 1996). Indeed, behavioral studies have verified that the combination of electric image amplitude and width provides a cue for object distance (von der Emde et al. 1998). Furthermore, a method for detecting small objects in the presence of a large background signal has been theoretically demonstrated (Babineau et al. 2007). For simple objects then, we have developed enough intuition about the input to the primary sensory afferents that we can properly address many questions regarding the neural mechanisms of object localization.

Our understanding of electric images, however, breaks down quickly as the complexity of the scene in question increases. The difficulties can be attributed to:

1. *The complexity of object arrangements within a scene.* The perturbing field of a simple object depends on the local electric field, which in turn depends on the other objects present. Each object thus interacts reciprocally with all the others, and the total perturbing field is not merely the sum of the perturbing fields of its constituent parts (Rother et al. 2003).
2. *The complexity of individual object geometries.* Individual objects can be considered as a collection of simple objects in the limits where their sizes and pairwise separations go to zero. Objects with dimensions of different length scales, such as a rod, are known to produce biphasic images when their longest axis is orientated parallel to the fish's rostral–caudal body axis. Also, the sharpness of edges and vertices of objects facing the skin have been shown to be in accordance with the sharpness of the associated mexican-hat-shaped image (Caputi and Budelli 2006).
3. *The presence of other field sources.* In contrast to the passive field perturbations caused by objects with conductivities different than that of the surrounding water, field sources, such as other fish or stimulation electrodes, are generally time-varying and thus produce electric images characterized by much more complicated spatiotemporal patterns (e.g. beats).

This last issue is the focus of the present study, because both temporal and spatial aspects of images due to another fish are known to be critical for electrosensory-mediated behaviors, such as the jamming avoidance response (JAR), but have yet to be well described. The JAR (Heiligenberg 1991) requires that a fish computes whether its EOD frequency is higher or lower than that of a neighboring fish, i.e. the sign of the difference frequency (dF), in order to modulate its frequency accordingly. A large body of behavioral data has shown that both temporal and spatial information are required for this computation (Heiligenberg 1991; Rose and Fortune 1999). In addition, electric fish often engage in complex physical interactions with conspecifics, as observed during territorial or courtship mediated encounters for example, and electrosensory inputs are a primary source of information during these interactions (Kramer and Bauer 1976; Moller 1976; Crockett 1986).

Describing the electric field of two interacting fish is a difficult task, however. Although one recent study (Aguilera et al. 2001) succeeded in systematically measuring the perturbation of a pulse-type fish's EOD near the snout, due to a conspecific at different locations, in general it is difficult to accurately map (in both space and time) the electric images of conspecifics. And so far, it has not been possible to do so during natural interactions.

Visualizing the electric field at high spatial and temporal resolutions, for the innumerable relative orientations of two fish, is thus now possible only with numerical models. To this end, we have developed a realistic 2-dimensional finite-element electric field model for the wave-type fish *Apteronotus leptorhynchus* (Babineau et al. 2006) that is amenable to the study of naturalistic electrosensory inputs. We have recently used this model to understand the inputs involved in prey detection (Babineau et al. 2007). In the present study, we extend our electric field model to investigate the electric images of a conspecific fish, and thus the spatial and temporal electrosensory consequences of two interacting conspecifics.

2 Methods — the conspecific interaction model

The development of a realistic conspecific interaction model consists of (1) developing a single fish model (2) calibrating the single fish model to experimental data and (3) applying the results to a two-fish model. The development of the single fish model has been previously described (Babineau et al. 2006), thus we focus on the last two steps in detail below, and emphasize that the third step, namely the development of a two fish model by extension of a single fish model, is not trivial.

2.1 Calibrating the single fish model to experimental field maps

The task of modeling an electric fish consists of solving Poisson's equation for the instantaneous electrostatic potential

Φ on domains of different conductivities, which represent the different components of the fish and the surrounding medium. Poisson's equation in 2-dimensions is

$$\sigma \nabla^2 \Phi(x, y) = -Q(x, y), \tag{1}$$

where σ is the conductivity of the given domain, Q is the current source density, and ∇^2 is the Laplace operator. Assuming that the fish and the surrounding medium are well modeled (i.e. their conductivities and geometry are known parameters) then calibrating the model to experimental data is an inverse problem that consists of finding a distribution of current sources (a source function Q) that reproduces the measured potential and the measured electric field (i.e. the negative gradient of the potential, $-\nabla\Phi$).

The calibration was performed with the model described in Babineau et al. (2006), which was designed to replicate accurately the experiment in which the potential and electric field maps were acquired (Assad 1997). The experimental setup consisted of a $70 \times 70\,\mathrm{cm}^2$ tank, grounded in one corner by an electrode, in which a 21 cm, 810 Hz fish was suspended immobilized. The insulating walls of the tank and the grounding electrode in the corner affect the boundary conditions to Poisson's equation and thus the electric field as well. By accounting for these conditions in the calibration, the solution obtained to the inverse problem (the source function Q) can then be applied to another model where the boundary conditions are symmetric about the fish, and the forward problem can be solved (i.e. computing the potential). This ensures that asymmetries in the ipsilateral/contralateral electric image are not confounded with asymmetries produced by the grounding electrode, for example. A flow chart summarizing this process, including the details below, is provided in Fig. 1.

The model fish consists of three domains of uniform conductivity (electric organ, body, and skin) and is surrounded by a third domain of uniform conductivity that represents the water. This differs slightly from the model used in the previous study (Babineau et al. 2006), where the skin conductivity differed by an order of magnitude in the head and tail, and varied linearly over the midbody (Assad 1997). This choice of skin conductivity was originally made because it reduced the error of the potential, but by using the fitting method that we describe below we discovered that a solution exists for a wide range of conductivity profiles, with insignificant differences in the errors of the associated potentials. We thus used a constant skin conductivity profile. Finally, the source function is defined only on the electric organ, and depends only on rostral–caudal position.

The procedure used to calibrate the model to the real field was based on the linearity of Poisson's equation. If two potentials are a solution to Poisson's equation, then so will be their sum, as long as the boundary conditions are the same in all cases. That is, if Φ_1 is the potential generated by the source function Q_1, and Φ_2 is the potential generated by the source function Q_2, then $\Phi_1 + \Phi_2$ is the potential generated by the source function $Q_1 + Q_2$.

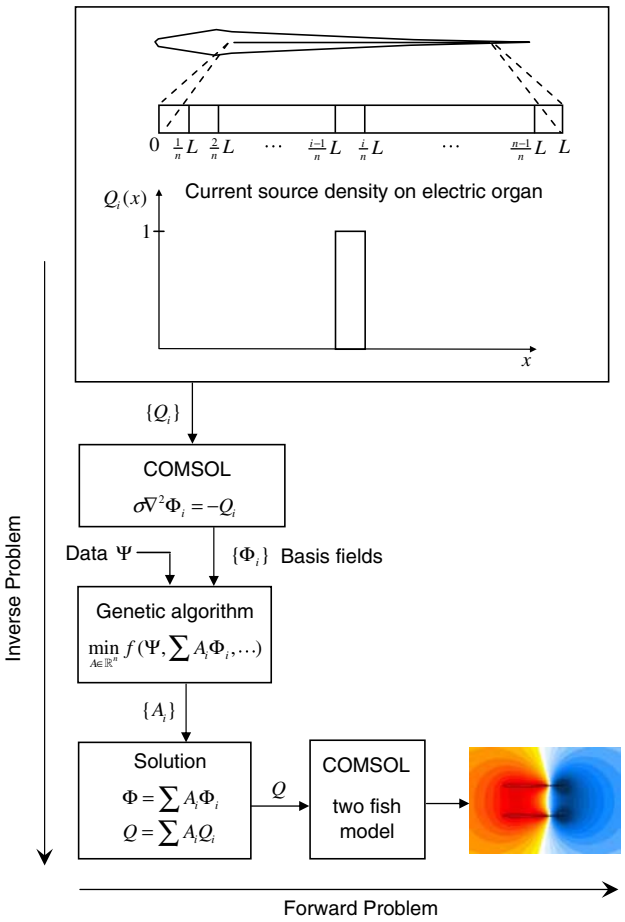

Fig. 1 A summary of the calibration process used to create a realistic conspecific interaction model. The inverse problem consists of finding a source function Q that reproduces the measured potential Ψ at a given phase in the EOD. The forward problem consists of applying solutions of the inverse problem to a two fish model and solving for the potential. (*Top to bottom*) Partition the electric organ into n segments; define each Q_i to be the indicator function over the ith segment; solve Poisson's equation for each Q_i and obtain a set of basis potentials $\{\Phi_i\}$; use a genetic algorithm to find the linear combination of the basis potentials which most closely reproduces the experimental potential, according to an objective function f (Eq. 4); the solution is a source function that is the same linear combination of the indicator functions. (*Bottom, Left to right*) Apply source functions that are solutions to the inverse problem to a two fish model; solve for the potential and predict the electrosensory consequences of two interacting conspecifics

Constructing electric fish models based on the principle of superposition is a well-established strategy (Bacher 1983; Chen et al. 2005). Thus, we partitioned the electric organ of the model fish into n segments, and defined the source function $Q_i(x)$ to be the indicator function of the ith segment

$$Q_i(x) = \begin{cases} 1 & \frac{i-1}{n}L \le x \le \frac{i}{n}L \\ 0 & \text{otherwise} \end{cases} \tag{2}$$

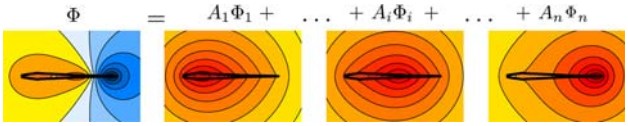

Fig. 2 The basis potentials. The potential of the real fish is assumed to be a linear combination of basis potentials. Refer to Fig. 1 for the definition of the basis potentials

where L is the length of the electric organ. We then computed the associated field Φ_i by solving Poisson's equation using finite-element-method software (COMSOL Inc., Burlington, MA), for each $i = 1 \ldots n$, and thus obtained a collection of basis potentials, $\{\Phi_i\}_{i=1\ldots n}$ (see Fig. 2).

We assumed the real potential Ψ to be a linear combination of these basis potentials. The associated source function is then the same linear combination of the n indicator functions. That is, equipped with experimental data for both the potential Ψ and the electric field $-\nabla\Psi$, we seek to find the linear combinations

$$\Phi = \sum_{i=1}^{n} A_i \Phi_i \qquad -\nabla\Phi = -\sum_{i=1}^{n} A_i \nabla\Phi_i \tag{3}$$

that best match the experimental maps. This can be rephrased as an optimization problem in which the task is to find the vector $A \in \mathbb{R}^n$ (whose components are the A_i's) that minimizes an objective function $f(\Psi, -\nabla\Psi, \Phi, -\nabla\Phi)$. We defined f to be the absolute difference between the electric fields and the potentials

$$f = |\nabla\Psi - \nabla\Phi| + \alpha\,|\Psi - \Phi|\,, \tag{4}$$

where α is a normalization constant required to similarly weight the electric field components and the potential, given by

$$\alpha = \frac{1}{2}\frac{\text{mean}(\|\nabla\Psi\|)}{\text{mean}(|\Psi|)}. \tag{5}$$

To solve this optimization problem we used a genetic algorithm (GA) (Chipperfield and Fleming 1995). In general, objective functions will have, by construction, a global minimum, but may also have many local minima. GA's are useful when little is known about the nature of the objective function because of their ability to avoid getting stuck in local minima, and are also effective at searching large parameter spaces. A GA is a biologically inspired optimization algorithm that begins with an initial population of individuals (a set of A vectors in our case) and creates successive populations according to rules analogous to the processes of natural selection, such as mutations and cross-overs. In this way solutions evolve towards optimal values. For a given data set (i.e. for a given phase of the EOD), we ran the GA 100 times, each time starting with a random initial population of 250 individuals, and selecting the fittest individual (the A vector that best minimizes) after 1000 iterations of the GA. We then averaged all the solutions.

2.2 The choice of n and the solution to the inverse problem

The value of n (i.e. the number of segments used to partition the electric organ) determines the resolution of the source function obtained by the GA, which is given by

$$Q = \sum_{i=1}^{n} A_i Q_i. \tag{6}$$

Although in general, inverse problems may not have unique solutions, the source function serves as a prediction for the net current density within the bounds of the rectangular electric organ used in the model. The source functions discovered in this study will be reported in a future study after further investigation into their biological implications.

The number of segments chosen was $n = 50$. There is a lower limit to the number of segments needed, below which the spatial variation of the fields obtained by a linear combination of the basis fields is too small to replicate the real fields. The upper limit is determined by the biophysical limit of discretization of the electric organ, given perhaps by the size and spacing of the electrocytes which compose the electric organ (Bennett 1971), but also on the ability to properly explore the $n-$dimensional parameter space (i.e. on computational resources).

2.3 Data used in the calibration

Both experimental potential and electric field maps were used in the calibration (Assad 1997). These maps comprised a total of 247 measurements made along seven lines of constant lateral distance away from the fish's rostral–caudal body axis, between approximately 1 and 14 cm. More measurements were taken at closer lateral distances from the fish, and thus the near field was implicitly weighted higher than the far field in the calibration (Assad 1997).

Although the electric field and potential were also measured near the fish's skin, these skin measurements were omitted from the data set used in the calibration. The amplitudes of the higher order temporal frequency components of the EOD decay rapidly with distance (Rasnow et al. 1993), and the amplitudes of the higher order spatial frequency components of the EOD, attributable to the higher order terms in the multipole expansion, also decay rapidly with distance. It follows that by omitting the skin measurements, both the temporal and spatial higher order frequency components are underweighted. The presence of certain higher order components can be attributed to complexities not included in our model. These include most importantly the differences in the body geometry of the real fish and the model fish.

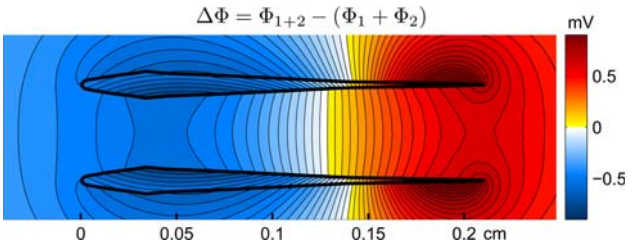

Fig. 3 An example of the difference $\Delta\Phi$ between the potential of two fish together Φ_{1+2} and the potential of each fish individually, Φ_1 and Φ_2. The difference is not negligible (compare with Fig. 7a, which shows Φ_{1+2}) and demonstrates the nonlinearity of a two fish model. Poisson's equation therefore needs to be solved for every different scenario. That is, the potential of two interacting fish cannot be calculated by a superposition of single fish potentials

For example, the real fish's tail was slightly bent during the experiment, while we modeled a fish with a symmetric body. The model fish also does not include the pectoral fins, which were shown to channel current dorsally (Rasnow and Bower 1996). Omitting the skin measurements also neglects the presence of local peaks and zero crossings along the skin, whose exact spatiotemporal patterns were shown to be unique to each fish.

2.4 Extending a single fish model to a two fish model

Although the above calibration procedure was based on the linearity of Poisson's equation, it is important to point out that it is not possible to model the interaction of two fish by simply adding the potentials of each fish, as obtained in a single fish model. Solutions to Poisson's equation with different boundary conditions are not superposable. Physically, this is because the presence of a second fish induces a charge distribution in the first (and vice-versa), which creates a new contribution to the total field. To quantify this, let the potential of one of the fish be Φ_1 (measured alone in a tank) and the potential of the other fish be Φ_2 (measured alone in the same tank). Then $\Phi_1 + \Phi_2$ is not equal to the potential of both fish together, Φ_{1+2}. The non-zero difference,

$$\Delta\Phi = \Phi_{1+2} - (\Phi_1 + \Phi_2),$$

gives a measure of the deviation from linearity. The example provided in Fig. 3 reveals that this deviation is not negligible.

Calculating the electric field of two interacting fish is thus not amenable to strategies based on a principle of superposition. For every different relative orientation of the two fish, and for every relative phase difference of their EODs, Poisson's equation must be solved. Technically, this is also true in the case of a single fish and a passive object. Although the total field is often assumed to be the sum of the fish's EOD, and the perturbing field that is produced by the given object when placed in a uniform field (e.g. a dipole), the reciprocal interaction of the object and the fish's body makes this invalid. However, the deviation from linearity in this case is usually assumed negligible, especially if the object is small (Lissmann and Machin 1958; Bacher 1983; Rasnow 1996).

3 Results of the calibration

We calibrated the single fish model to three phases of the EOD of a 21 cm, 810 Hz *Apternotus leptorhynchus*, using the electric field and potential maps acquired by Chris Assad (Assad 1997). The first phase selected (referred to as phase 1) is near the positive peak of the EOD (130°), the second phase selected (phase 2) is near the zero crossing of the EOD (187°), and the third phase selected (phase 3) is near the negative peak of the EOD (288°). Phase 1 and 3 are biphasic, while phase 2 is triphasic (with respect to position along the rostral-caudal body axis). The simulated EOD phases are compared to the measured EOD phases in Fig. 4.

The errors for each phase are reported in Table 1, calculated according to

$$\text{Error} = \frac{1}{n}\sum_{i=1}^{n} |\Phi_i - \Psi_i| \tag{7}$$

which represents the average difference per measurement. The maximum and minimum measurement values are also reported in Table 1 for scale.

It is important to realize, however, that the discrepancy between the potential computed by our model and the potential of the real fish are on the same order as the variations observed between individual fish. It was reported (Rasnow and Bower 1996) that the major differences in the fields of individual fish included the absolute amplitude, and the exact spatiotemporal pattern of the EOD potential on their body. Emphasis should be placed, therefore, on the qualitative similarities between the potentials.

4 The electric image of a conspecific

When two fish with different EOD frequencies interact, the potential at a given point in space will be some amplitude modulated waveform (i.e. characterized by beats). The potential in space will be further modulated by the motion of each fish. In general, then, the beat pattern will not be periodic. Even in the case of two stationary fish with stable EODs, the beat pattern will not be strictly periodic because the higher frequency components of the beat will not all be integer multiples of the fundamental (Rasnow et al. 1993). That is, consecutive beats will differ slightly. At any given phase within a beat cycle, the potential in space, and more importantly the electric images on each fish, will be characterized by spatial

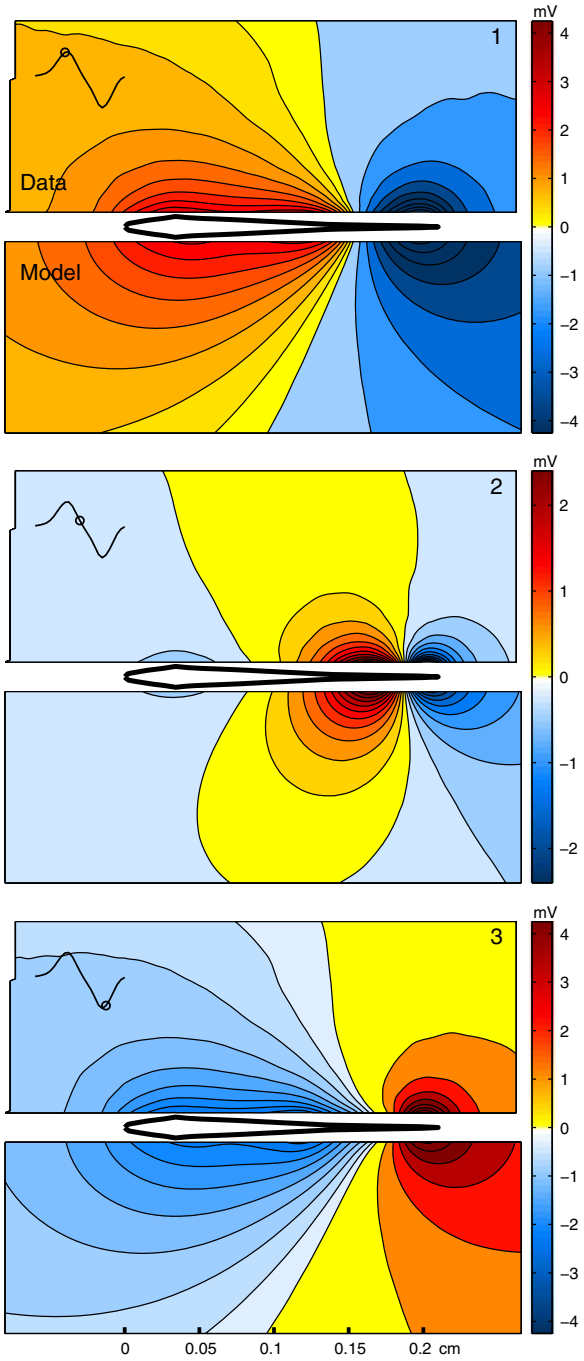

Fig. 4 Experimental (*upper panel*) and model (*lower panel*) potential maps of the three EOD phases for which the single fish model was calibrated. Phase 1 is near the positive peak of the EOD (130°), phase 2 is near the zero crossing of the EOD (187°), and phase 3 is near the negative peak of the EOD (288°). The inset on each upper panel shows the head-tail waveform with the corresponding EOD phase indicated by an open circle. Phase 1 and 3 are biphasic, while phase 2 is triphasic (with respect to position along the rostral-caudal body axis). The potential maps were measured for a 21 cm, 810 Hz *Apteronotus leptorhynchus* by Chris Assad (Assad 1997). Note that the constant of proportionality between the potential line density and the electric field intensity (gradient of the potential) differs between the positive and negative regions to facilitate comparison of the experimental and model data sets. See Methods for details on the calibration procedure

Table 1 Error of calibration and range of data

	Error (mV)	Min (mV)	Max (mV)
Phase 1	0.6124	−8.3722	3.0635
Phase 2	0.2052	−2.8570	2.8528
Phase 3	0.5488	−2.5885	8.9131

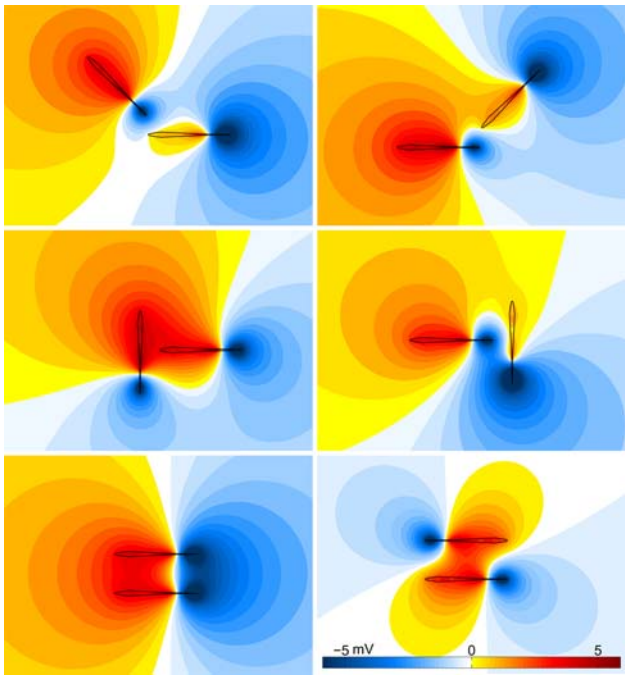

Fig. 5 Potential maps generated by the two fish model for several possible orientations of two interacting fish, each at a fixed phase (130°, phase 1) of their EOD. Each fish measures 21 cm in length

patterns that depend on the relative orientation of the fish, and on the particular phase within the beat cycle. To give an appreciation for the qualitative features of the electric fields that result from the interaction of two fish, the potential maps for several possible orientations of two fish are displayed in Fig. 5.

In order to study the spatial and temporal patterns that appear in the electric image of a conspecific, we studied three phases (referred to as phase A, B and C) within half of a beat cycle, for fish in two relative orientations, parallel and perpendicular. The three phases within the beat cycle were modeled by applying to the two fish model combinations of the three selected EOD phases (see previous section). The three combinations are A = (1, 1), B = (1, 2), and C = (1, 3). In other words, the EOD phase of one of the fish (referred to as the receiver fish) does not change, while the other fish (referred to as the sender fish) cycles through the three selected EOD phases.

In Fig. 6, an example is constructed to illustrate, in terms of the standard head-tail potential differences, where these

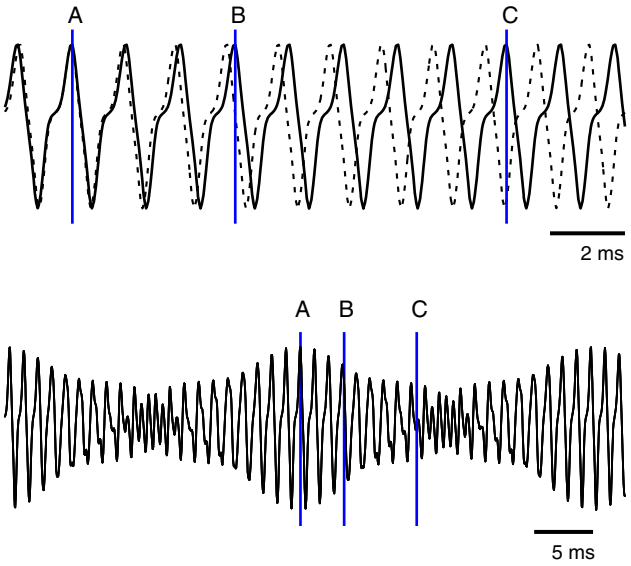

Fig. 6 An example constructed to illustrate the choice of the three EOD phases calibrated, and the combinations studied in the two fish model. (*Top*) The EOD of the receiver fish (810 Hz, *solid line*, real data) and the EOD of the sender fish (850 Hz, *dashed line*) measured as a head-tail potential difference. The markers indicate where in each of the fish's EOD the selected combinations of phases occur. (*Bottom*) The sum of the two EODs in the top figure. The markers indicate where in the resulting beat the selected combinations of phases occur. Note that the addition of the two fish's head–tail potential is illustrative and not physically meaningful due to the nonlinearity of two interacting fish (see Fig. 3)

combinations occur within each fish's individual EOD and within the beat cycle. Thus, if the receiver fish is sampling its environment at its EOD frequency, then this example represents three non-consecutive samples made during the positive peak of its EOD. The potential maps and the electric images on the receiver fish for phases A, B and C are shown in Fig. 7 in the case that the sender fish is oriented parallel to the receiver fish, and in Fig. 8 for the case that the sender fish is oriented perpendicular to the receiver fish.

In both the parallel and perpendicular orientations, the symmetry of the positive peak and negative peak phases of the sender fish's EOD is faithfully represented in the electric image on the receiver fish (A and C). In the parallel orientation, the ipsilateral (same side as the sender fish) and contralateral (opposite side as the sender fish) images have very similar spatial profiles (A and C), but are of opposite polarity, and the amplitude of the contralateral image is approximately half of the amplitude of the ipsilateral image. This is also true in the perpendicular orientation, but the spatial profiles of the ipsilateral and contralateral images differ significantly (Fig. 8). The contralateral images are very uniform, with no zero crossings, while the ipsilateral images contain a peak that corresponds to the location of the sender fish.

In the perpendicular orientation, the transition from A to B to C (which corresponds to the decreasing half of the modulation envelope in a beat cycle) predicts that the electric image waveforms at fixed points along the ipsilateral side are all approximately in phase, but differ in amplitude, whereas the electric image waveforms at fixed points along the contralateral side are all approximately identical.

In the parallel orientation (Fig. 7), both the spatial profiles and the temporal progression of the electric images differ significantly from those in the perpendicular orientation; the intermediate phase is biphasic (B). That is, there is a change in polarity near the midbody and the images, both ipsilateral and contralateral, contain a peak and a trough. The contralateral image for phase (B), however, lags that of the ipsilateral image; *this reveals an ipsilateral/contralateral phase difference*. The transition from A to B to C predicts that the electric image waveforms at fixed points along both the ipsilateral and contralateral sides are all not in phase, and *that the phase differences vary smoothly rostrocaudally*.

5 Mimicking conspecifics by optimizing the stimulation paradigm

The neuronal processing of communication-like signals in weakly electric fish has been studied extensively in recent years (Bastian et al. 2002; Chacron et al. 2003; Doiron et al. 2003). These studies use a two-electrode transverse stimulation geometry to mimic communication signals and have interpreted their results accordingly. The question of what, exactly, this stimulation paradigm mimics is one that has not been properly addressed, and there is evidence to suggest that the placement of the stimulation electrodes affects the fish's behavioral response (Rose et al. 1988). Computational models such as ours, however, can clarify the information present with different electrode configurations. Thus, we examined this problem using our model by asking the following question: *how should two stimulation electrodes be placed to best mimic the electric image of a conspecific in a given orientation?* To answer this question, we computed the electric image of a conspecific for two orientations (parallel and perpendicular), then used a Nelder-Mead downhill simplex algorithm (an optimization algorithm that does not use numerical or analytic gradients) (Lagarias et al. 1998) to find the placement and amplitude of the electrodes which best matches simultaneously both the ipsilateral and contralateral electric images of the fish. In Fig. 9, the results are compared to the electric image produced by the common transverse stimulation, placed 10 cm laterally and 10 cm caudally to the fish, and also optimized over the amplitude to match the ipsilateral electric image of the conspecific.

The major differences between the electric image due to the transverse stimulation and the electric image due to the realistic stimulations are: (1) the transverse stimulation

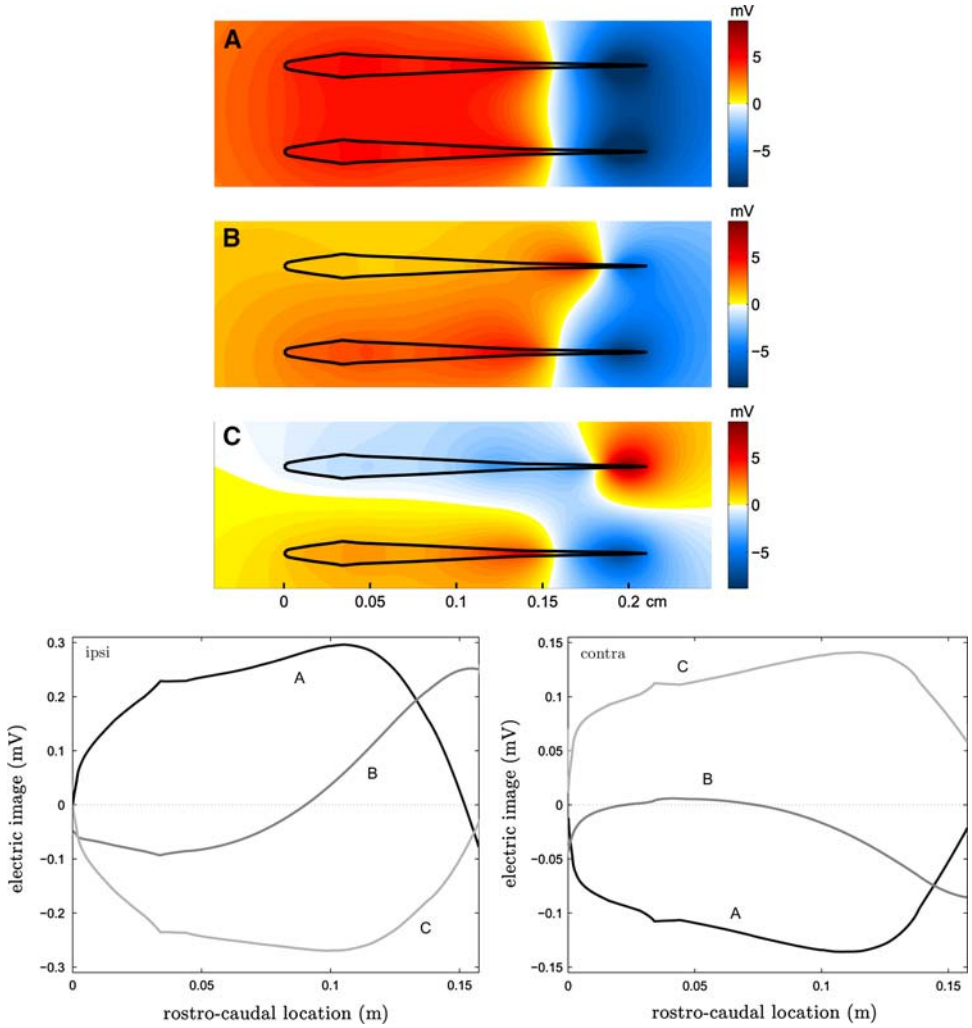

Fig. 7 (*Top*) The potential maps for fish in a parallel orientation, at three phases of the decreasing half of a beat (A to B to C). The receiver (*bottom*) fish's EOD phase is constant to represent sampling by electroreceptors near the positive peak of the EOD. (*Bottom*) The electric images on the receiver fish at the same three phases of the beat. Both ipsilateral and contralateral electric images are shown

produces identical (although of opposite polarities) ipsilateral and contralateral images whereas this is not true in general for a conspecific in any orientation and; (2) the transverse stimulation produces electric images of constant polarity, whereas in general a conspecific produces images with spatial variations in polarity (e.g. the biphasic image in Fig. 7).

The conclusion is the following: given the objective to produce a naturalistic stimulus by mimicking the electric image of a conspecific, and given that this is to be accomplished via a dipolar stimulation in the midplane of the fish, and further assuming the only free parameters are the dipole amplitude A, the dipole separation d, the dipole rotation ϕ, and the dipole's position r (relative to some fixed coordinate system), then there exists a set of values (A, d, ϕ, r) for which the dipole stimulation produces an electric image practically indistinguishable (to the experimenter) from that of a real fish. *Yet, this is not the common transverse arrangement used to mimic a conspecific*. This conclusion is not surprising, for it was already shown that there are dipole orientations that produce a greater magnitude JAR (Rose et al. 1988), namely when the dipole axis is not perpendicular to the fish's rostral–caudal body axis. The electric image of such an off-perpendicular transverse stimulation is biphasic (data not shown), similar to the biphasic image produced by a parallel conspecific (Fig. 7).

We have shown that a dipole stimulation best mimics a conspecific in a given orientation when it is oriented parallel to the fish, is located along the rostral-caudal axis of the fish, and has a separation approximately the length of the fish. The converse, then, may also be true: the fish that is mimicked by the dipole stimulation is one that is oriented parallel to the dipole axis. The separation and amplitude of the dipole thus controls the size and amplitude of the mimic. These conclusions are in hindsight quite obvious: weakly electric fish are approximately dipoles, so a dipole with the same dimensions of a fish should best produce a naturalistic stimulus.

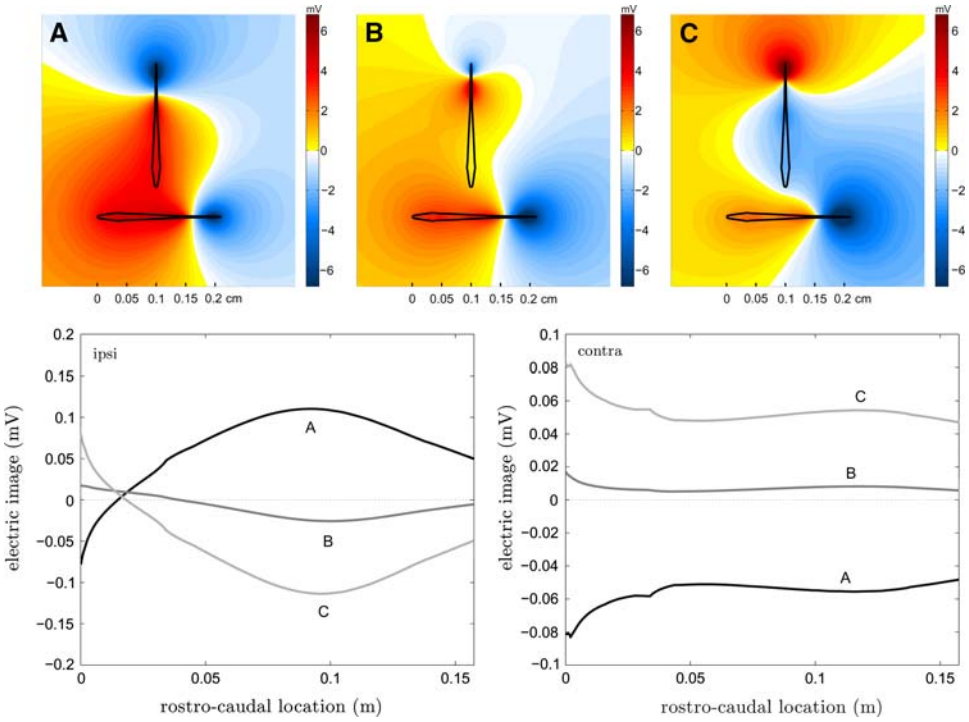

Fig. 8 (*Top*) The potential maps for fish in a perpendicular orientation, at three phases of the decreasing half of a beat (A to B to C). The receiver (bottom) fish's EOD phase is constant to represent sampling by electroreceptors near the positive peak of the EOD. (*Bottom*) The electric images on the receiver fish at the same three phases of the beat. Both ipsilateral and contralateral electric images are shown

6 Discussion

6.1 Localizing conspecifics

It has long been argued that sufficient information is available in the EOD modulation caused by another fish to enable it to be localized (Heiligenberg and Bastian 1984). Furthermore, it appears necessary that the modulations at multiple points along the body must be sampled for unambiguous localization. In a study on pulse-type fish (Aguilera et al. 2001) measurements were made of the electric field perturbations at the head region due to conspecifics at various orientations and distances. It was found that many orientations resulted in a similar perturbation. However, one position produced a unique perturbation (the nearest anti-parallel orientation tested). Although localization ability may be compromised if based on information from the head-region alone, it may still be possible for a limited set of positions.

The electric images we describe provide direct evidence that sufficient electrosensory information is available for conspecific localization; the temporal variation of the electric image over a beat cycle is systematically related to relative fish position and orientation (Figs. 7 and 8). This is in agreement with previous speculation (Heiligenberg and Bastian 1984). The electric image of a conspecific in a perpendicular orientation is qualitatively akin to a standing disturbance, while the electric image of a conspecific in a parallel orientation is qualitatively akin to a propagating disturbance. Although we have only shown detailed electric images for two particular fish positions, it is clear that different fish positions will result in different spatial patterns (both rostral/caudal and ipsilateral/contralateral) of amplitude and phase modulations. In principle, localization accuracy could be estimated quantitatively (in terms of the quality of the sensory information available), but this is beyond the scope of the present study.

6.2 Implications for eliciting the JAR

The same amplitude and phase variations that could in principle provide information for conspecific localization are known to underlie the neural computations required for the jamming avoidance response, JAR (Heiligenberg 1991). A landmark series of studies, using stimulations of various geometries and temporal patterns, showed clearly that in order for a fish to determine whether to increase or decrease its own frequency during a JAR, it must compare the amplitude and phase modulation of its EOD over different spatial locations (Heiligenberg et al. 1978; Rose and Heiligenberg 1986; Heiligenberg 1991; Rose and Fortune 1999). When EOD modulations do not vary spatially, no JAR results.

In this study we explicitly show what natural EOD modulations look like for two relative fish positions (Figs. 7, 8). In particular, we show how the amplitude and phase modulations over the length of the body will depend on relative fish orientation, so one might expect that the strength of the JAR might also depend on fish position. Indeed, using transverse electrodes at an off-perpendicular angle to the rostral–caudal

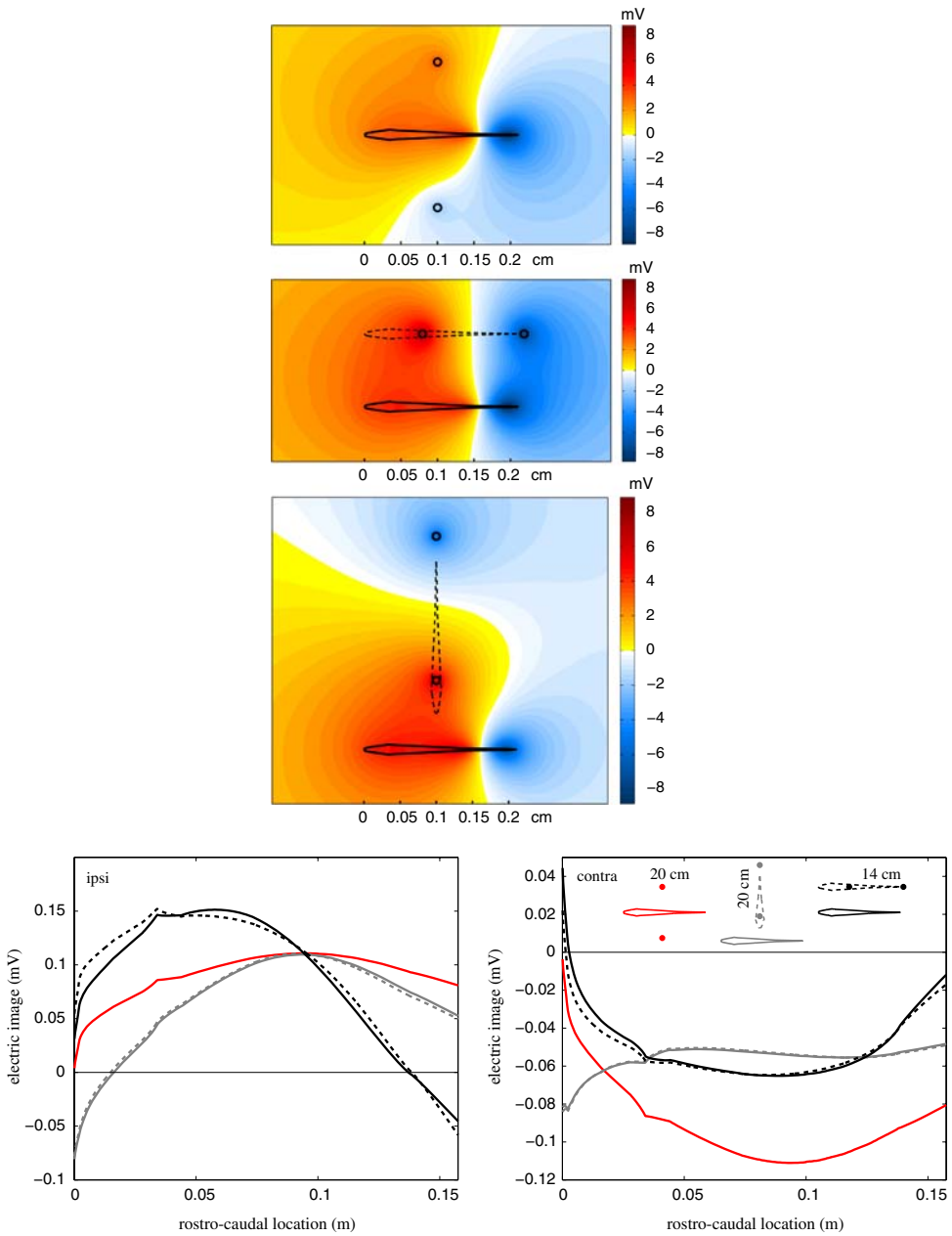

Fig. 9 Mimicking a conspecific with a dipole stimulation; the common transverse stimulation paradigm compared to a more realistic stimulation paradigm. (*Top*) Potential maps: transverse stimulation, realistic stimulation optimized to mimic a perpendicular conspecific, and realistic stimulation optimized to mimic a parallel conspecific. The position of the conspecific fish being mimicked is shown by the *dashed outline*. (*Bottom*) Ipsilateral and contralateral electric images corresponding to the three top panels: dipole stimulation (*solid lines*) versus conspecific (*dashed lines*); transverse stimulation (*red line*), perpendicular conspecific (*gray line*), and parallel conspecific (*black line*)

body axis was found to be more effective at eliciting the JAR (Rose et al. 1988). This also suggests the interesting possibility that during aggressive encounters, a dominant fish may actively orient itself to more effectively influence other fish.

Our results also point to an explanation for how a moving object may induce a JAR (Carlson and Kawasaki 2007). If an object produces an electric image that has sufficient amplitude and width (e.g. a large, conductive object at a sufficient lateral distance), then as it moves along the side of the body, it may produce a pattern of amplitude and phase modulations similar to those shown in Fig. 7). This intriguing possibility must be further investigated, both in the context of the appropriate stimulus and the associated behavior.

6.3 Experimental mimics of conspecific fish

Many studies of electrosensory processing have taken advantage of the convenience with which electric signals can be delivered. Most have utilized a dipole stimulus geometry, with the two electrodes positioned transversely across the fish's rostral–caudal body axis. Some of the original JAR experiments used the transverse geometry (Heiligenberg et al. 1978). In addition, different variations of the transverse geometry were used to show that the JAR required both amplitude and phase variations (Partridge et al. 1981; Rose et al. 1988; Rose and Heiligenberg 1986; Heiligenberg and Bastian 1984).

More recent studies have also used the transverse stimulation geometry to simulate the “global" (i.e. spatially diffuse) signals of a conspecific (Chacron et al. 2003; Bastian et al. 2002; Doiron et al. 2003). Our results suggest that such a stimulation geometry, although useful experimentally, and sufficiently sophisticated to evoke responses consistent with the presence of another fish, do not adequately mimic naturalistic stimuli (Fig. 9). These discrepancies should not impact the responses of individual electroreceptors, because they respond to local changes in EOD amplitude. However, some care should be taken when interpreting the responses of any neurons in the subsequent points of the electrosensory processing stream that integrate over different spatial locations. It is not clear whether neurons in the first central nucleus (electrosensory lateral line lobe, ELL), are sensitive to stimulation geometry. It has been suggested (Partridge et al. 1981) that ELL pyramidal neurons were not sensitive to stimulus orientation (using a circular transverse electrode array), but more recent studies have shown that the response properties of these neurons can be influenced by stimuli outside of their receptive field (Chacron et al. 2003). Nonetheless, stimulus geometry will surely be important for studying higher level processing, in the torus for example, where neurons are known to be tuned to stimulus orientation and motion (Ramcharitar et al. 2006; Partridge et al. 1981; Rose et al. 1988).

While we stress the importance of using more realistic stimulation geometry, it may be difficult in practice to implement accurate signal-mimics with a dipole stimulation. It is theoretically possible to optimize the electrode orientation, as we have shown, but in practice the optimal values will depend on the experimental setup (tank size, fish size, water conductivity, etc.), and on the nature of the problem (what is being mimicked). In the future, it may prove more effective to use more elaborate stimulation geometries, based on arrays of electrodes for example.

6.4 Limitations of the 2D model

One possible limitation of our approach is that we use a 2-dimensional model of an inherently 3-dimensional problem, and it is unclear how the results change when extrapolated to 3D. However, for a large part of the mid-body our model performs very well because (1) the fish body is such that the lateral skin surface is relatively flat, i.e. the dorsal axis is much longer that the lateral axis, and (2) the dorsal component of the electric field is relatively small. Near the head and the tail however, where the body tapers, the 2-dimensional approach is less accurate (Babineau et al. 2007).

Furthermore, our model has yet to be experimentally tested, and so its accuracy is still under question. The model contains several free parameters for which a proper sensitivity analysis has not been performed, and whose values are based on assumptions which have not been experimentally verified in any rigorous way, such as the skin conductivity profile.

6.5 Spatiotemporal patterns in the electric images of a conspecific: future work

Although the number of possible combinations of phases studied here is small, our results reveal patterns in the electric images of a conspecific in the form of spatially varying amplitude and phase differences that depend on the position and orientation of the conspecific and on the phase of the beat cycle. These patterns are apparent in both rostral/caudal and ipsilateral/contralateral variations in the images. The goal of the present study was to characterize a small sample of possible images due to a conspecific, but a greater understanding of their spatiotemporal patterns can be achieved by modeling a beat cycle to a higher temporal resolution. It is possible, as we have shown, that the patterns in the images due to a conspecific contain localizing information, with regards to both position and orientation. It is thus also possible that electric fish communicate different messages based on their relative orientation. Future studies will allow us to quantify the associated spatiotemporal images and formulate specific hypotheses that can then be tested in behavioral experiments. Such an experiment may involve, for example, using an optimized time-varying dipole mimic to reliably invoke reactions in a receiver fish consistent with natural predictive responses to the position and orientation of a sender fish.

References

Aguilera PA, Castello ME, Caputi A (2001) Electroreception in gymnotus carapo: differences between self-generated and conspecific-generated signal carriers. J Exp Biol 204:185–198

Assad C (1997) Electric field maps and boundary element simulations of electrolocation in weakly electric fish. Pasadena, CA: California Institute of Technology; University Microfilms Inc, Ann Arbor, MI

Babineau D, Longtin A, Lewis JE (2006) Modeling the electric field of weakly electric fish. J Exp Biol 209:3636–3651

Babineau D, Lewis JE, Longtin A (2007) Spatial acuity and prey detection in weakly electric fish. PLoS Comp Biol 3:e38

Bacher M (1983) A new method for the simulation of electric fields, generated by electric fish, and their distortions by objects. Biol Cybern 47:51–58

Bastian J, Chacron MJ, Maler L (2002) Receptive field organization determines pyramidal cell stimulus-encoding capability and spatial stimulus selectivity. J Neurosci 22:4577–4590

Bennett M (1971) Electric Organs. In: Fish physiology, Academic Press, New York, pp 347–491

Caputi A, Budelli R (2006) Peripheral electrosensory imaging by weakly electric fish. J Comp Physiol A 192:587–600

Carlson BA, Kawasaki M (2007) Behavioral responses to jamming and ‘phantom’ jamming stimuli in the weakly electric fish Eigenmannia. J Comp Physiol A 193:927–941

Chacron MJ, Doiron B, Maler L, Longtin A, Bastian J (2003) Non-classical receptive field mediates switch in a sensory neuron's frequency tuning. Nature 423:77–81

Chen L, House JL, Krahe R, Nelson ME (2005) Modeling signal and background components of electrosensory scenes. J Comp Physiol A 191:331–345

Chipperfield A, Fleming P (1995) The matlab genetic algorithm toolbox. IEE Colloquium on Applied Control Techniques Using MATLAB 1995/014:10

Crockett D (1986) Agonistic behavior of the weakly electric fish, Gnathonemus petersii. J Comp Physiol 100(1):3–14

Doiron B, Chacron MJ, Maler L, Longtin A, Bastian J (2003) Inhibitory feedback required for network oscillatory responses to communication but not prey stimuli. Nature 421:539–543

von der Emde G (1999) Active electrolocation of objects in weakly electric fish. J Exp Biol 202:1205–1215

von der Emde G, Schwarz S, Gomez L, Budelli R, Grant K (1998) Electric fish measure distance in the dark. Nature 395:890–894

Heiligenberg W (1991) Neural nets in electric fish. MIT Press, Cambridge, MA

Heiligenberg W, Bastian J (1984) The electric sense of weakly electric fish. Ann Rev Physiol 46:561–583

Heiligenberg W, Baker C, Matsubara J (1978) The jamming avoidance response in Eigenmannia revisited: the structure of a neuronal democracy. J Comp Physiol 127:267–286

Kramer B, Bauer K (1976) Agonistic behaviour and electric signalling in a mormyrid fish, Gnathonemus pertersii. Behav Ecol Sociobiol 1:45–61

Lagarias J, Reeds J, Wright M, Wright P (1998) Convergence properties of the Nelder-Mead simplex method in low dimensions. SIAM Journal of Optimization 9(1):112–147

Lissmann H, Machin K (1958) The mechanism of object location in Gymnarchus niloticus and similar fish. J Exp Biol 35:451–486

Moller P (1976) Electric signals and schooling behavior in a weakly electric fish, Marcusenius cyprinoides l. (Mormyriformes). Science 193:697–699

Partridge B, Heiligenberg W, Matsubara J (1981) The neural basis of a sensory filter in the jamming avoidance response: no grandmother cells in sight. J Comp Physiol 145:153–168

Ramcharitar JU, Tan EW, Fortune ES (2006) Global electrosensory oscillations enhance directional responses of midbrain neurons in Eigenmannia. J Neurophysiol 96:2319–2326

Rasnow B (1996) The effects of simple objects on the electric field of Apteronotus. J Comp Physiol A 178:397–411

Rasnow B, Bower JM (1996) The electric organ discharges of the gymnotiform fishes: I. Apteronotus leptorhynchus. J Comp Physiol A 178:383–396

Rasnow B, Assad C, Bower JM (1993) Phase and amplitude maps of the electric organ discharge of the weakly electric fish, Apteronotus leptorhynchus. J Comp Physiol A 172:481–491

Rose G, Heiligenberg W (1986) Limits of phase and amplitude sensitivity in the torus semicircularis of Eigenmannia. J Comp Physiol A 159:813–822

Rose G, Kawasaki M, Heiligenberg W (1988) Recognition unit at the top of a neuronal hierarchy? prepacemaker neurons in Eigenmannia code the sign of frequency differences unambiguously. J Comp Physiol 162:759–772

Rose GJ, Fortune ES (1999) Mechanisms for generating temporal filters in the electrosensory system. J Exp Biol 202:1281–1289

Rother D, Migliaro A, Canetti R, Gomez L, Caputi A, Budelli R (2003) Electric images of two low resistance objects in weakly electric fish. Biosystems 71:171–179